Journal of Controlled Release 307 (2019) 379–392

Contents lists available at ScienceDirect

Journal of Controlled Release

journal homepage: www.elsevier.com/locate/jconrel

Influence of size and charge of unstructured polypeptides on pharmacokinetics and biodistribution of targeted fusion proteins

Fabian Brandl[a,b], Hannes Merten[a], Martina Zimmermann[a], Martin Béhé[c], Uwe Zangemeister-Wittke[a,b,*], Andreas Plückthun[a,*]

[a] Department of Biochemistry, University of Zurich, Winterthurerstrasse 190, CH-8057 Zurich, Switzerland
[b] Institute of Pharmacology, University of Bern, Inselspital INO-F, CH-3010 Bern, Switzerland
[c] Center of Radiopharmaceutical Sciences, Paul Scherrer Institute, CH-5232 Villigen PSI, Switzerland

ARTICLE INFO

Keywords:
DARPin
PASylation
XTENylation
Half-life extension
Biodistribution
Tumor targeting

ABSTRACT

Alternative non-IgG binding proteins developed for therapy are small in size and, thus, are rapidly cleared from the circulation by renal filtration. To avoid repeated injection or continuous infusion for the maintenance of therapeutic serum concentrations, extensions of unfolded polypeptides have been developed to prolong serum half-life, but systematic, comparative studies investigating the influence of their size and charge on serum half-life, extravasation, tumor localization and excretion mechanisms have so far been lacking. Here we used a high-affinity Designed Ankyrin Repeat Protein (DARPin) targeting the tumor marker epithelial cell adhesion molecule (EpCAM) in a preclinical tumor xenograft model in mice, and fused it with a series of defined unstructured polypeptides. We used three different sizes of two previously described polypeptides, an uncharged one consisting of only Pro, Ala and Ser (termed PAS) and a charged one consisting of Pro, Ala, Ser, Thr, Gly, Glu (termed XTEN) and performed for the first time a precise comparative localization, distribution and extravasation study. Pharmacokinetic analysis showed a clear linear relationship between hydrodynamic radius and serum half-life across both polypeptides, reaching a half-life of up to 21 h in mice. Tumor uptake was EpCAM-dependent and directly proportional to half-life and size, showing an even tumor penetration for all fusion proteins without unspecific accumulation in non-target tissue. Unexpectedly, charge had no influence on any parameter, neither tumor nor tissue accumulation nor kidney elimination kinetics. Thus, both polypeptide types have a very similar potential for precise half-life modification and tumor targeting.

1. Introduction

Numerous biopharmaceuticals based on alternative non-IgG protein scaffolds have been developed for cancer therapy. Most of these therapeutic proteins are small, with sizes below the renal filtration threshold, causing rapid elimination from the circulation [1–4] and thus a short serum half-life. To avoid infusion or repeated injections of the proteins to maintain high serum concentrations, various strategies to extend the short serum half-life of therapeutic proteins have been developed.

One such approach is to increase the hydrodynamic radius of the protein and thus its size above the renal filtration threshold. Most popular has been the chemical conjugation of polymers such as polyethylene glycol (PEG) [5,6]. However, PEG-molecules show a high polydispersity leading to molecules with a broad size distribution [7,8], making batch-to-batch consistency and half-life optimization difficult. Besides, PEG must be coupled to the therapeutic protein by chemical conjugation via engineered reactive sites [9], requiring additional steps in product development and analysis, and making reproducibility more

Abbreviations: ABD, albumin binding domain; aSEC, analytical size exclusion chromatography; AUC, area under the curve; BV, blood volume; CL, clearance; DARPin, Designed Ankyrin Repeat Protein; DMSO, dimethyl sulfoxide; ECFV, extracellular fluid volume; EpCAM, epithelial cell adhesion molecule; EPR, enhanced permeability and retention; ESI-MS, electrospray ionization mass spectroscopy; FcRn, neonatal Fc receptor; Her2, human epidermal growth factor receptor 2; HRV-3C protease, human rhinovirus 3C protease; *i.v.*, intravenous; IDP, intrinsically disordered protein; IMAC, immobilized metal ion affinity chromatography; MIP, maximum intensity projection; MW, molecular weight; MW_{app}, apparent molecular weight; Ni-NTA, nickel nitrilotriacetic acid; PEG, polyethylene glycol; PTS, portable test system; scFv, single-chain Fv fragment; SD, standard deviation; SEC-MALS, size exclusion chromatography coupled to multi-angle light scattering; sfGFP, superfolder green fluorescent protein; SPECT, single-photon emission computer tomography; SPR, surface plasmon resonance; TEV protease, tobacco etch virus protease; V_d, volume of distribution

* Corresponding authors at: Department of Biochemistry, University of Zurich, Winterthurerstrasse 190, CH-8057 Zurich, Switzerland.
E-mail addresses: uwe.zangemeister@pki.unibe.ch (U. Zangemeister-Wittke), plueckthun@bioc.uzh.ch (A. Plückthun).

https://doi.org/10.1016/j.jconrel.2019.06.030
Received 28 May 2019; Received in revised form 22 June 2019
Available online 25 June 2019
0168-3659/

challenging. PEG is not biodegradable; it accumulates in various tissues and can induce cellular and renal tubular vacuolation [10,11], and neutralizing anti-PEG antibodies have been reported in patients treated with PEGylated biopharmaceuticals [12], which can lead to its rapid clearance from the circulation [13].

Another frequently used strategy for half-life extension is to exploit the natural recycling mechanism of the neonatal Fc receptor by coupling the therapeutic protein to serum albumin, to serum albumin binding domains [14,15] or to the Ig-Fc domain [16–18]. Hitchhiking the endosomal FcRn-recycling pathway was shown to be more effective than merely increasing the protein size, and both approaches can be combined to get an increased effect [19,20]. On the other hand, this approach cannot be used for tuning a product to give it predictable intermediate pharmacokinetics. However, this would be desirable for therapeutics with systemic toxicity, where an optimum between targeting efficiency and off-target effects must be found.

Recently, two types of intrinsically disordered proteins have been reported to increase hydrodynamic volume and reduce elimination by renal filtration. The first type is uncharged and consists only of the amino acids Pro, Ala, Ser (termed PAS) [21], while the second type is negatively charged and consists of Pro, Ala, Ser, Thr, Gly, Glu (termed XTEN) [22]. They can be genetically fused to any therapeutic protein to give monodisperse fusion constructs of strictly defined sizes [23,24] and thus unique pharmacokinetic profiles. PAS and XTEN have been reported as non-immunogenic in several mammalian species and described as fully biodegradable without inducing accumulation and vacuolation in cells, and therefore they may be better tolerated than PEG-derived conjugates [21,22].

Despite their conceptual similarity, PAS and XTEN greatly differ in charge and amino acid composition, from which one might expect different pharmacological behavior, notably in repulsion from cell membranes of target or non-target tissues, or from excretion organs. So far, a side-by-side comparison of different lengths/sizes of the two polypeptides under fully identical in vivo conditions has not been conducted, with respect to serum half-life, extravasation, tumor localization, accumulation in non-targeted healthy tissue or excretion mechanisms.

To clarify these effects, we made use of a Designed Ankyrin Repeat Protein (DARPin) that targets the epithelial cell adhesion molecule (EpCAM) on tumor cells with picomolar affinity [25,26], and the unstructured polypeptides were fused to this DARPin. DARPins are a class of small non-IgG binding proteins characterized by unique robustness, giving much freedom for engineering, ease of production in *E. coli* and favorable biophysical and biochemical properties [27–31]. For tumor targeting, DARPins binding to various tumor-selective cell surface receptors with high affinity and specificity have been developed and characterized [25,32–41].

In different preclinical models we had demonstrated that, due to their small size, DARPins and DARPin-toxin constructs have very short serum half-lives of only several minutes [37,39,40], and that PEGylation [36,40] improves tumor targeting by half-life extension.

Here we used a DARPin that binds to EpCAM as a model system to engineer proteins by fusion to the intrinsically disordered polypeptides PAS or XTEN of different defined lengths (300, 600, 900 aa for PAS and 288, 576, 864 aa for XTEN) to systematically determine the effects of size and charge on serum half-life, tumor and tissue accumulation and excretion mechanism. As initially their expression and purification was found to be not straightforward, we developed a robust generic expression and purification protocol for these proteins. We report here a systematic comparative investigation of the pharmacokinetics in mice, the relationship to charge and hydrodynamic radius, as well as the levels of unspecific uptake by non-tumor tissues and excretion mechanisms. Our findings describe the factors that influence pharmacokinetics and biodistribution and thereby help optimize the desired modulation of a given binding protein by design.

2. Materials and methods

2.1.1. Construction of XTEN and PAS sequences

The PAS sequences were constructed based on the PAS#1-repeat sequence [21]. PAS-sequences of three different lengths (PAS#, # = 300, 600, 900 amino acid residues) were assembled by sequential combination of PAS#100 segments, consisting of multiple PAS#1-repeats, which were codon-optimized for *E. coli* expression and gene-synthesized (Geneart), each bearing unique restriction sites. The 5′ (first) and 3′ (last) PAS#100 segments always carried 5′ *Bmt*I and 3′ *Bam*HI restriction sites for further cloning steps.

The original XTEN864 amino acid sequence was extracted from ref. [22]. XTEN-sequences of three different lengths (XTEN#, # = 864, 576, 288 amino acid residues) were designed from the original XTEN864 sequence. The XTEN576 consisted of the first 576, while the XTEN288 sequence consisted of the last 288 amino acids of the XTEN864 sequence, respectively. DNA sequences with 5′ *Bmt*I and 3′ *Bam*HI restriction sites were constructed, codon optimized for *E. coli* expression and gene-synthesized (Geneart).

2.1.2. Cloning of polypeptide-DARPin fusion proteins

The plasmid pQIq encoding the EpCAM-binding DARPin Ec1 [33] was modified (Fig. 1A) at the DARPin 5′ end by introducing a gene fragment encoding for superfolder green fluorescent protein (sfGFP) [42], a TEV cleavage site (ENLYFQG) and a FLAG™-tag (DYKDDDDK) including a *Bmt*I restriction site at the 3′ end. PAS and XTEN sequences were introduced between the FLAG™-tag and the DARPin by cloning via *Bmt*I and *Bam*HI restriction sites. For IMAC purification, a C-terminal HRV-3C protease cleavable His_6-tag (LEVLFQGPGSHHHHHH) was fused to the DARPin 3′ end. GFP-tagged PASylated and XTENylated DARPins were under the control of a T5 promoter (Fig. 1A). For non-binding control fusion proteins, DARPin Ec1 was replaced by DARPin Off7 [43], recognizing the *E. coli* maltose binding protein.

2.1.3. Expression and purification of polypeptide-DARPin fusion proteins

Chemically competent *E. coli* BLR (DE3) (Novagen) cells were transformed with the pQIq plasmids encoding PASylated and XTENylated fusion proteins of the DARPins Ec1 and Off7. Overnight cultures consisting of 2-YT medium supplemented with 1% (*w/v*) glucose and 100 µg/mL ampicillin were inoculated with a single colony. After shaking for 16 h at 37 °C, 1 L ZYM-5052 auto-inducing medium [44] supplemented with 100 µg/mL ampicillin was inoculated with 20 mL overnight culture. The expression cultures were grown at 37 °C for 2 h, subsequently the temperature was lowered to 25 °C. After 22 h, the cultures were centrifuged (4000 x *g*, 10 min, 4 °C) and washed by resuspension of the cell pellets in ice-cold PBS pH 7.4. Cell pellets were resuspended in 50 mM Tris-HCl pH 8.0, 400 mM NaCl (TBS400), supplemented with 3 mg/mL lysozyme, 100 µg/mL DNase I and lysed by sonication and French Press. The resulting lysates were centrifuged (21′000 x *g*, 30 min, 4 °C) and the supernatants applied to Ni-NTA Superflow (Qiagen) metal affinity columns (20–60 mL resin). All columns were washed with each 15 column volumes (CV) of 50 mM Tris-HCl pH 8.0, 20 mM imidazole supplemented with 400 mM NaCl, 1 M NaCl or 20 mM NaCl, respectively. Proteins were eluted in 5 CV PBS pH 7.4, 500 mM imidazole. Next, the eluted proteins were applied to 5 mL GFP affinity-columns [45] and washed with each 15 CV of TBS400 and 15 CV TBS400 supplemented with 5 mM ATP, 5 mM $MgCl_2$ to remove bound DnaK. The GFP affinity-columns were equilibrated with 50 mM Tris-HCl pH 8.0, 150 mM NaCl, 0.5 mM EDTA, 1 mM DTT and TEV protease produced in-house was added to a final concentration of 100 µg/mL. After incubation overnight at 4 °C, the cleaved proteins were eluted and concentrated by ultrafiltration (Amicon Centrifugal Filter Units, Millipore). Concentrated proteins were polished by preparative size exclusion chromatography on an Äkta Explorer FPLC

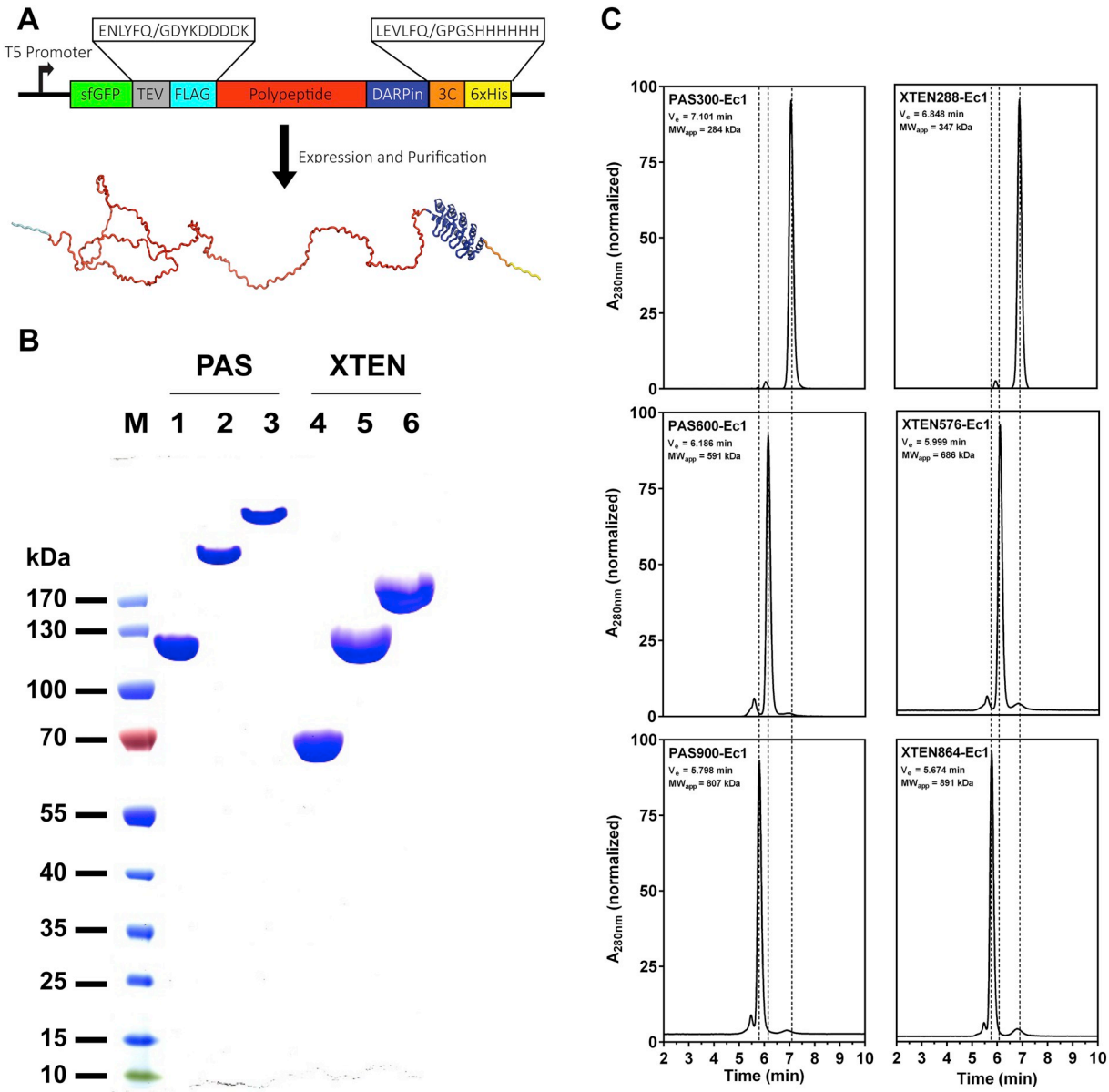

Fig. 1. Design and characterization of PASylated and XTENylated DARPin Ec1. A) Schematic representation of expression constructs and a Rosetta-simulated exemplary model of the final protein construct of a 300 aa fusion. B) SDS-PAGE of purified proteins as used for in vivo experiments. Lane 1) PAS300-Ec1, 2) PAS600-Ec1, 3) PAS600-Ec1, 4) XTEN288-Ec1, 5) XTEN576-Ec1, 6) XTEN864-Ec1. C) Analysis of proteins by analytical SEC-HPLC for determination of apparent molecular size.

system (GE Healthcare) using a Superose 6 Increase 10/300 GL (GE Healthcare) column and PBS pH 7.4 as running buffer. Fractions containing the desired proteins were pooled and concentrated by ultrafiltration (Amicon Centrifugal Filter Units, Millipore). Proteins were snap-frozen and stored at −80 °C.

2.1.4. SDS-PAGE analysis

Equimolar amounts (113 pmol) of protein were analyzed by non-reducing SDS-PAGE using NuPAGE™ 4–12% Bis-Tris Protein Gels (Thermo Fisher Scientific) with NuPAGE™ MOPS SDS running buffer (Thermo Fisher Scientific). As molecular weight standard PageRuler™ Prestained Protein Ladder (Fermentas) was used. Gels were stained with Coomassie Brilliant Blue R250 (Sigma-Aldrich).

2.1.5. Analytical gel filtration

PASylated and XTENylated DARPins were analyzed on an Agilent Advanced BioSEC column (Agilent) connected to an Agilent 1260 Infinity Bio-inert Quaternary LC HPLC system (Agilent). Ten microliters of 10 µM protein dilutions in PBS pH 7.4 were injected to the HPLC system at a flow rate of 0.35 mL/min. The elution profiles were monitored by absorbance at 280 nm. For calculation of apparent molecular weights, an injection of a high molecular weight gel filtration standard (Agilent) was included.

2.1.6. Binding kinetics by surface plasmon resonance spectroscopy

The binding kinetics of PASylated and XTENylated DARPin Ec1 to the purified extracellular domain of human EpCAM (hEpEx) were determined on a ProteOn™ XPR36 instrument (BioRad). The ligand protein hEpEX was expressed, purified and enzymatically biotinylated as previously described [39]. First, two ligand channels of a NeutrAvidin-functionalized chip (ProteOn™ NLC Sensor Chip, BioRad) were coated with 500 RU of biotinylated hEpEX in PBS-TE (PBS pH 7.4, 0.005% Tween 20, 3 mM EDTA). Following a buffer injection for baseline stabilization, a serial dilution of the polypeptide-DARPin fusion proteins

(81 nM - 0.33 pM) was injected on separate ligand channels in duplicates. The flow rate of all steps was 60 μL/min, the association time and the dissociation time were 400 s and 2500 s, respectively. The chip surface coated with ligand was regenerated between analyte runs by two bursts of 25 μL 100 mM H_3PO_4 for 25 s. The sensorgrams were double referenced by subtraction of interspot signals and a blank analyte channel. Data was fitted to a 1:1 Langmuir binding model and analyzed using the ProteOn™ Manager Software (Version 3.1.0.6, BioRad).

2.1.7. ESI-MS and SEC-MALS

Mass determination was done by electrospray ionization mass spectroscopy at the Functional Genomics Center Zurich (FGCZ) and by size exclusion chromatography coupled to multi-angle light scattering (SEC-MALS). For SEC-MALS, proteins were analyzed on an LC1100 HPLC system (Agilent) coupled to an Optilab rEX refractometer (Wyatt Technology) and a miniDAWN three-angle light scattering detector (Wyatt Technology). Proteins were separated in a Superose 6 10/300 GL column (GE Healthcare) with a flow rate of 0.5 mL/min in PBS pH 7.4.

2.1.8. Endotoxin removal

For endotoxin removal, purified proteins were applied to an EndoTrap HD (product discontinued, Hyglos GmbH) affinity resin according to the manufacturer's instructions. The buffer of eluted protein was exchanged to endotoxin-free Dulbecco's PBS (Millipore) by PD-10 desalting columns (GE Healthcare). Endotoxin content was determined with an EndoSafe Portable Test System (Charles River Laboratories) using PTS test cartridges with 0.5–0.005 EU/mL sensitivity. The amount of endotoxin in all purified samples was always below 5 EU/mg of protein.

2.1.9. Mice

Female Crl:CD1-*Foxn1*^{nu} mice aged 6–8 weeks were purchased from Charles River Laboratories and kept under sterile conditions according to the guidelines of the veterinary ordinance of the Kanton Zürich for animal welfare.

2.1.10. Pharmacokinetics – blood clearance in mice

For measurement of in vivo blood clearance, mice were injected i.v. into the tail vein with 4.5 mg/kg of PAS300/600/900-Ec1 or XTEN288/576/864-Ec1 (N = 5 mice per group). Blood samples were drawn from the saphenous vein at defined time points (for PAS300-Ec1 and XTEN288-Ec1, 3 min, 1, 3, 6, 9, 12 and 24 h, and for PAS600/900-Ec1 and XTEN576/864-Ec1, 3 min, 1, 3, 6, 12, 24 and 48 h post injection). After blood coagulation at room temperature for 30 min, serum was prepared by two centrifugation steps (coagulated blood 7 min 3100 x *g*, serum 3 min 5000 x *g*, room temperature) and stored at −80 °C until quantification of serum concentrations by ELISA. Briefly, black 384-well Immuno Plates (Thermo Fischer Scientific) were coated with 20 μL mouse anti-$(H)_4$ monoclonal antibody (Qiagen) at a dilution of 1:1000 in PBS pH 7.4 at 4 °C overnight. The wells were blocked for 1 h at at 30 °C in a temperature-controlled atmosphere with 300 μL PBS-TB (PBS pH 7.4, 0.2% BSA, 0.1% Tween-20).

A serial dilution of serum samples ranging from 1:50 to 1:800 was prepared by 1:1 dilution in PBS-TB. Two dilutions of each sample were applied to coated wells. Control wells were incubated with PBS-TB spiked with the respective dilution of CD1 nude serum for background subtraction. For quantification of serum concentrations, serial dilutions of purified polypeptide-DARPin fusions were prepared ranging from 50 nM to 390 pM. Standard dilutions were prepared in PBS-TB supplemented with 0.125% to 2% (v/v) serum from an untreated animal to ensure an identical composition of the sample matrix. Twenty microliters of the serum samples or the standard dilution were applied to coated and blocked wells. The plate was incubated for 1 h at 30 °C. The wells were washed three times with PBS-T (PBS pH 7.4, 0.1% Tween-20) at RT and incubated for 1 h at 30 °C with 20 μL of a 1:5000 dilution of rabbit anti-DARPin polyclonal antibody (custom-made, Eurogentec) in PBS-TB. After another washing step with PBS-T, 20 μL of a 1:10,000 dilution of goat anti-rabbit IgG (whole molecule)-peroxidase antibody (Sigma-Aldrich) in PBS-TB were applied to the wells. Incubation of the plate for 1 h at 30 °C was followed by four final washing steps with PBS-T.

The assay was developed using Amplex UltraRed (Invitrogen). A 10 mM Amplex UltraRed solution in DMSO was diluted 1:400 in 75 mM Na-citrate pH 6.0 and 20 μL were added to each well for detection. Fluorescence was measured using a BioTek Synergy HT plate reader (BioTek Instruments). All standards were prepared in triplicates (N = 3) and each data point was measured in quadruplicates (N = 4). Serum samples were measured in at least two dilutions on different plates and every data point was measured in quadruplicates (N = 4). The standard curve spiked with mouse serum and the corresponding diluted serum sample for quantification were always on the same ELISA microplate. Non-linear regression using a 4PL-model was used to fit the data from serial dilutions to obtain a standard curve (Graph Pad Prism Version 6.07, GraphPad Software Inc.). Concentrations of the recombinant proteins in the serum samples were quantified by interpolation of measured data points with the standard curves.

Data fitting and calculation of pharmacokinetic parameters with a two-compartment model (2-phase exponential decay) was performed using GraphPad Prism 6 (Version 6.07, GraphPad Software Inc.). The area under the curve (AUC) was calculated by integration of a two-compartment model describing the distribution and elimination of i.v. injected polypeptide-DARPin fusion proteins. Clearance (CL), elimination rate constant (k_e) and apparent volume of distribution (V_d) were calculated with the formulas: $CL = D/AUC$, $k_e = \ln(2)/\tau^{\beta}_{1/2}$, $V_d = CL/k_e$, where D is the dose, $\tau^{\beta}_{1/2}$ is the terminal half-life, and k_e is the elimination rate constant.

2.1.11. Tumor cells

The EpCAM-positive colon adenocarcinoma cell line HT29 was obtained from DSMZ (German Collection of Microorganisms and Cell Cultures) and cultured in Dulbecco's Modified Eagle's medium (DMEM). Cell culture medium was supplemented with 10% (v/v) heat-inactivated fetal calf serum (Amimed) and 1% (v/v) Penicillin-Streptomycin (Sigma-Aldrich). The cells were tested for human and murine pathogens (IDEXX BioResearch) and cultivated at 37 °C in a humidified atmosphere containing 5% CO_2.

2.1.12. Tumor xenografts

Tumor xenografts were established on the back or the right shoulder of mice by subcutanous injection of 8×10^6 HT29 cells. Experiments started 2–4 weeks after tumor cell inoculation when tumors reached an average volume of 100 mm^3. Tumors were measured two times per week with calipers and the volume was calculated according to the formula: (short diameter)^2 x (long diameter) x 0.4.

2.1.13. His-tag-specific [^{99m}Tc](CO)$_3$-labeling of DARPin-fusion proteins

His-tag-specific radiolabeling of DARPin-fusion proteins with [^{99m}Tc](CO)$_3$ was performed as described previously [46]. Carbonyl labeling Isolink kit vials (Mallinckrodt Medical B.V.) containing lyophilized sodium tartrate (8.5 mg), sodium borate decahydrate (2.85 mg), sodium carbonate (7.15 mg) and sodium boranocarbonate (4.5 mg) were used to prepare [^{99m}Tc$(H_2O)_3(CO)_3]^+$, abbreviated as [^{99m}Tc](CO)$_3$. Technetium pertechnetate ($^{99m}TcO_4^-$) was freshly eluted from a 10.75 GBq UltratechneKow® FM Technetium Generator (Mallinckrodt Medical B.V.) and added to the Isolink vial (1 mL). The vial was placed into an organic synthesis microwave oven and heated for 40 s at 150 °C. The solution was neutralized by adding 350 μL of a buffer mixture of pH 6.5, containing 2 parts of 1 M HCl and 3 parts of 0.6 M phosphate buffer pH 7.0. Proteins were mixed with the required amount of radioactivity and incubated for 1 h at 37 °C with agitation.

Prior to injection to mice, the degree of radioactive labeling was analyzed by reversed phase C18 HPLC chromatography connected to an HPLC radioactivity monitor.

2.1.14. Biodistribution of radiolabeled DARPins

Mice were injected i.v. into the tail vein with a single dose of 413 pmol [^{99m}Tc](CO)$_3$-labeled (1.0–3.0 MBq/mouse) DARPin-fusion protein in a volume of 100 µL. After 1, 4, 24 and 48 h mice (N = 3 mice per time point and construct) were sacrificed, organs were excised and the accumulated radioactivity was measured in a γ-scintillation counter. The total activity injected was set to 100% and the measured accumulated radioactivity in each organ and time point was normalized to the percentage of injected dose per gram of tissue (%ID/g).

2.1.15. Single photon emission computer tomography (SPECT)

Mice (N = 2) were injected i.v. into the tail-vein with 532 pmol of [^{99m}Tc](CO)$_3$-labeled DARPin-fusion protein with 7.5 MBq. Twenty-two to twenty-four hours after injection, mice were anesthesized with isoflurane and imaged in a NanoSPECT/CT device (Bioscan) with a 4-head multiplexing multi-pinhole camera. For highest resolution, pinholes with 1.0 mm diameter and a thickness of 10 mm were used. The acquisition time was always set to 2:05 h to obtain comparable images. CT scans were collected using the integrated CT with a tube voltage of 45 kVp. After the image acquisition, SPECT data were reconstructed with the HiSPECT Software (Bioscan) and fused with the CT images. Images were then analyzed with the InVivoScope postprocessing software (Bioscan).

2.1.16. Organ autoradiography

After SPECT imaging, mice were sacrificed and tumors, right kidney and liver were excised and frozen in OCT embedding matrix (Cell Path). Frozen tissues were cut into 5 µm thick slices using a cryostat microtome (Bright Instruments), transferred to Superfrost Plus™ microscope slides (Thermo Fisher Scientific) and air-dried. The microscope slides were placed on super-resolution or multisensitive storage phosphor screens (Perkin Elmer) and screens were imaged with a Cyclone® Plus Storage Phosphor System (Perkin Elmer) after 16 h. Images were processed using Adobe Photoshop CC 2018 (version 19.1.3).

3. Results

3.1.1. Construction of generic polypeptide-DARPin fusion proteins

To investigate the influence of charge and molecular size on serum half-life, biodistribution and secretion, we created a series of fusion proteins to the EpCAM-binding DARPin Ec1 [33], which has an affinity of 88 pM (Table 1). We created matching sets of fusions to intrinsically disordered peptides with and without negative charge, short (PAS300/XTEN288), intermediate (PAS600/XTEN576) and long (PAS900/XTEN864), where the number indicates the number of fused amino acids. The sequences were generated either by repetitive ligation of the PAS#1 repeat [21] or by full gene synthesis of published XTEN sequences [22]. We fused the PAS or XTEN polypeptides of varying length to the N-terminus of DARPin Ec1 and the non-binding control DARPin Off7 (Fig. 1A).

3.1.2. Preparation of extraordinary pure polypeptide-DARPin fusion proteins

Initial experiments had shown some smear on SDS gels, indicating some incomplete synthesis in *E. coli* and/or partial degradation of these long unstructured proteins, compounded by unsatisfactory purification results. To overcome these problems, all proteins were expressed in the cytoplasm of *E. coli* BL21 BLR (DE3) [47], a *rec*A deficient strain to reduce the risk of recombination of highly repetitive polypeptide sequences and to thus keep the expression plasmids stable (Fig. 1A). We then developed a three-step purification protocol which resulted in highly pure, homogeneous and full-length proteins, despite their great size and unusual properties (Fig. 1B). As the first step, all proteins were purified by immobilized metal ion affinity chromatography (IMAC), using a hexahistidine-tag, which had to be placed at the C-terminus, thereby yielding already almost pure full-length protein preparations. Next, to enrich only full-length proteins with an intact N-terminus, their N-terminal sfGFP-tag was bound to an anti-GFP-affinity column, carrying a very tight-binding immobilized "wrap-around" anti-GFP DARPin [45]. All proteins without an N-terminal GFP-tag were washed off the column. The bound full-length DARPin fusion proteins were subsequently cleaved off the column-bound GFP by addition of tobacco etch virus (TEV) protease, using an engineered cleavage site. After elution, followed by an additional polishing step by size exclusion chromatography (SEC), highly pure and monodisperse protein preparations were obtained as shown by SDS-PAGE and analytical size exclusion chromatography (Fig. 1 B,C). Bacterial endotoxin was subsequently removed by lipopolysaccharide affinity purification to achieve endotoxin levels below 1 EU/mL protein for in vivo use. Typical final purification yields from 1 L *E. coli* shake flask culture were 30–50 mg for both polypeptide-DARPin fusion types (PAS and XTEN).

3.1.3. Biochemical and biophysical characterization of purified proteins

SDS-PAGE (Fig. 1B) confirmed highly pure protein preparations without any traces of co-purified *E. coli* proteins or degradation, and Western blotting confirmed the presence of N-terminal FLAG™- and the C-terminal His$_6$-tag and the absence of any other band (Fig. S1). As previously shown by others [21,22], proteins fused to hydrophilic peptides migrate more slowly than expected from the molecular weight, probably due to reduced binding of SDS to the polypeptide chains,

Table 1
Biophysical characterization of PASylated and XTENylated and unmodified EpCAM-binding DARPin Ec1.

Construct	MW_{calc} [a] (kDa)	MW_{abs} [b] (kDa)	MW_{app} [c] (kDa)	Diameter [d] (nm)	k_{on} [e] ($M^{-1}\,s^{-1}$)	k_{off} [e] (s^{-1})	K_D [e] (M)
Ec1	19.30	19.30	29	N.A.	1.39×10^5	1.22×10^{-5}	8.78×10^{-11}
PAS300-Ec1	44.92	44.92	284	8.3	7.09×10^4	1.27×10^{-5}	1.79×10^{-10}
PAS600-Ec1	69.49	69.49	591	11.6	4.69×10^4	9.09×10^{-6}	1.94×10^{-10}
PAS900-Ec1	94.05	94.05	807	14.8	4.69×10^4	1.10×10^{-5}	2.53×10^{-10}
XTEN288-Ec1	46.93	46.93	347	8.3	5.62×10^4	7.90×10^{-6}	1.41×10^{-10}
XTEN576-Ec1	73.21	73.21	686	11.8	5.54×10^4	6.00×10^{-6}	1.08×10^{-10}
XTEN864-Ec1	99.63	99.64	891	15.0	5.63×10^4	7.82×10^{-6}	1.39×10^{-10}

[a] Molecular weights were calculated (MW_{calc}) with the ProtParam tool on the ExPASy server based on the amino acid sequence of polypeptide-DARPin fusion constructs.
[b] The absolute molecular weight (MW_{abs}) was determined by ESI-MS.
[c] Apparent molecular weights (MW_{app}) were determined by analytical size exclusion chromatography on an HPLC system.
[d] Diameters were determined by size exclusion chromatography coupled to multi-angle light scattering.
[e] Binding kinetics to EpCAM (hEpEx) was determined by surface plasmon resonance spectroscopy (SPR).

which negatively charges the protein for electrophoretic separation. PASylated DARPins always migrated less on SDS-PAGE than their respective negatively charged XTENylated counterparts. For example, PAS300-Ec1 and XTEN288-Ec1 have a calculated molecular weight of 44.9 kDa and 46.9 kDa, but migrated as 120-kDa and 70-kDa proteins, respectively.

Electrospray ionization mass spectrometry (ESI-MS) confirmed the masses of all purified polypeptide-DARPin fusion proteins (Fig. S2) and matched the calculated molecular weights (Table 1). Multi-angle light scattering coupled to size exclusion chromatography (SEC-MALS) confirmed the ESI-MS determined masses and showed that the protein samples were monodisperse, with a polydispersity index of Mw/Mn = 1.0 (Table ST1).

To investigate the different effect of fusing uncharged PAS and charged XTEN polypeptides on hydrodynamic volume, analytical gel filtration (SEC-HPLC) was performed (Fig. 1C) and the apparent molecular size was calculated from MW standards (Table 1). The proteins eluted early from the gel filtration column, indicating a large hydrodynamic radius, equivalent to an apparent molecular size of approx. 280 kDa up to 879 kDa for PAS300-Ec1 and XTEN288-Ec1, and PAS900-Ec1 and XTEN864-Ec1, respectively (Table 1). Thus, PASylation and XTENylation of the DARPin increased its average apparent size at least 10- to 30-fold, from 29 kDa [28,33,37,38] of the unmodified DARPin.

It is well known that the modification of binding proteins with polymers such as PEG can alter the binding kinetics by a small reduction of the association rate constant [48], due to transient intramolecular blocking of the paratope, as well as intermolecular blocking after binding on a target surface. This was also observed with the polypeptide fusions investigated here when measured with surface plasmon resonance (SPR) on a biosensor chip coated with biotinylated extracellular domain of EpCAM (hEpEX) (Table 1). The unmodified DARPin association rate constant decreased by about a factor two, from $1.39 \times 10^5\,M^{-1}\,s^{-1}$ to an average of $5.54 \times 10^4\,M^{-1}\,s^{-1}$, in the fusions, similar to PEGylation [48]. On the other hand, the dissociation rate constants (k_d) of the polypeptide-DARPin fusion proteins were not affected by fusion to PAS and XTEN polypeptides within the error of the measurements (Table 1, Fig. S3), again as has been observed for PEGylation [48]. As a consequence, the equilibrium dissociation constants (K_D) increased slightly, from 1.2 to 2.9-fold, yet no clear trend for length, type or overall negative charge was observed. In other words, the high affinity of the DARPin Ec1 was maintained in the fusion proteins.

3.1.4. Pharmacokinetics of DARPins shows linear relationship of hydrodynamic volume and serum half-life, across both polypeptides

While the polypeptide-DARPin fusion proteins can be expected to be cleared from the circulation more slowly, similar to PEG conjugates, it was important to investigate the effect of charge and defined size in a systematic in vivo side-by-side comparison of PASylated and XTENylated proteins under identical conditions, as effects of charge on excretion organs and/or interaction with serum or endothelial components might occur and might lead to non-linear behavior. For this purpose, anti-EpCAM DARPin Ec1, fused to PAS or XTEN of three defined lengths, was injected i.v. into mice. Blood was collected at various time points and serum concentrations were determined by a carefully calibrated sandwich ELISA to calculate and compare all relevant pharmacokinetic parameters (Fig. 2A, Table 2).

The serum concentration time courses of all PAS- and XTEN-DARPin fusion proteins followed a bi-exponential decay with a short initial distribution phase (α-phase) and a long terminal elimination phase (β-phase) (Fig. 2A). Compared with the short half-life of only about 11 min for DARPin Ec1 [37], fusions with PAS and XTEN polypeptides strongly extended the terminal half-life to between 5.3 and 20.6 h (30- to 114-fold), depending on the polypeptide length and type.

Interestingly, DARPin fusion proteins with XTEN always showed slightly longer terminal elimination half-lives than their comparable PAS counterparts (Table 2), even though the latter comprise somewhat fewer amino acids in the matched pairs. When relating the hydrodynamic volumes to the terminal half-lives of all fusion proteins, a linear relationship was observed (Fig. 2B) across both classes of fusions. This indicates that the serum half-life is directly correlated only with

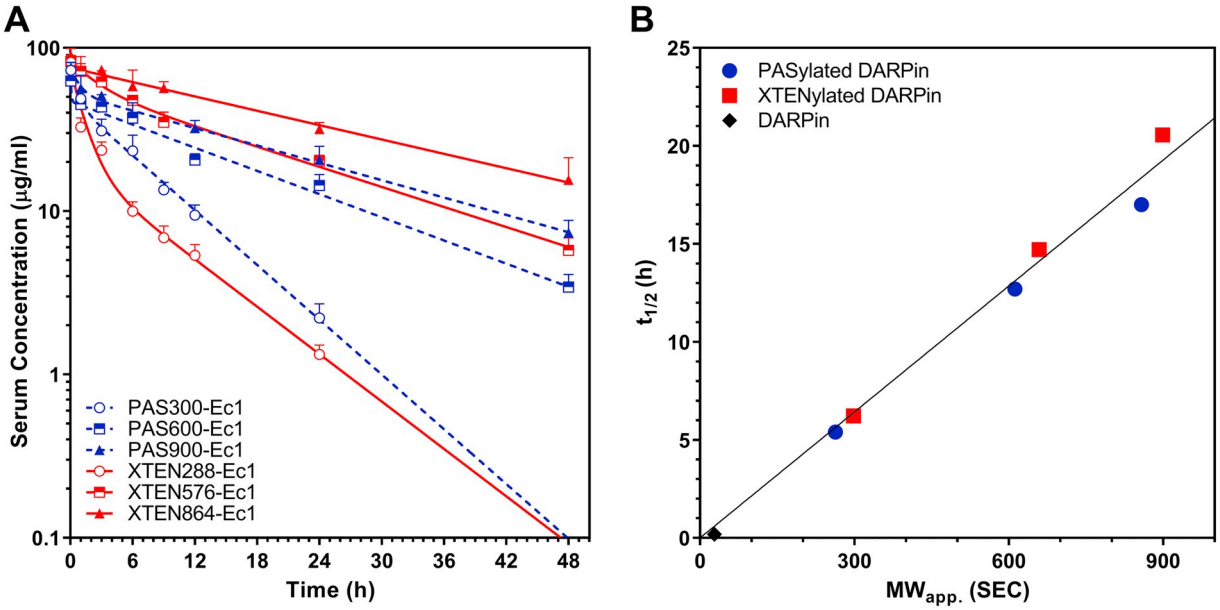

Fig. 2. In vivo pharmacokinetics of PASylated and XTENylated DARPin Ec1. A) Blood clearance of PASylated and XTENylated DARPin. All proteins were injected i.v. into mice at 4.5 mg/kg. Blood samples were collected 3 min, 1, 3, 6, 9, 12 and 24 h for PAS300-Ec1 and XTEN288-Ec1, and 3 min, 1, 3, 6, 12, 24, 48 h for all other constructs after injection. Serum concentrations of the fusion proteins were quantified by sandwich ELISA and interpolation with an appropriate protein standard. Data points are the average ± SD of $N = 5$ mice, and each measured in two different dilutions. Data were fitted with GraphPad Prism version 6.07 using a pharmacokinetic two-compartment model (bi-exponential decay). B) Linear relationship of serum half-life ($\tau^{\beta}_{1/2}$) and apparent molecular size (MW_{app}) determined by analytical size exclusion chromatography (aSEC-HPLC).

Table 2
Pharmacokinetics of PASylated and XTENylated EpCAM-binding DARPin Ec1.[a]

Construct	$\tau^{\beta}_{1/2}$ [b] (h)	AUC [c] (h µg/mL)	CL [d] (mL h^{-1})	k_e [b] (h^{-1})	V_d [d] (mL)
PAS300-Ec1	5.39	379	0.317	0.129	2.46
PAS600-Ec1	12.72	856	0.140	0.054	2.57
PAS900-Ec1	17.00	1167	0.103	0.041	2.52
XTEN288-Ec1	6.22	245	0.490	0.111	4.40
XTEN576-Ec1	14.71	1222	0.098	0.047	2.08
XTEN864-Ec1	20.55	1825	0.066	0.034	1.95

[a] Parameters were calculated after i.v. injection in mice using GraphPad Prism Version 6.07. Elimination half-lives are averages of the 95% confidence interval of $N = 5$ mice.

[b] Terminal serum elimination half-life ($\tau^{\beta}_{1/2}$) and elimination rate constant k_e were calculated by fitting the data with a 2-phase exponential decay function.

[c] The area under the curve (*AUC*) was calculated by integration of the 2-phase exponential decay function from the first sampling time point to the last sampling time point.

[d] Clearance rate (*CL*) and apparent volume of distribution (V_d) were determined by calculation from $CL = D/AUC$ or $V_d = CL/k_e$, where D is the dose.

the hydrodynamic volume and essentially independent of the charge of the polypeptide type used. The increased elimination half-lives of the polypeptide fusion proteins also resulted in increased areas under the curve (AUC), which ranged from 245 to 1825 h µg/mL and gave rise to decreased clearance rates (CL) of 0.5 to 0.07 mL h^{-1} (Table 2).

The apparent volume of distribution (V_d) is used as a measure for the extent of equilibration and distribution of an injected compound within the body tissues after injection. Mice have an extracellular fluid volume (ECFV) and a blood volume (BV) of approx. 21% and 7.5% of the body weight, respectively [49]. Considering the body weight of the mice, this corresponded to approx. 6 mL ECFV and 2 mL BV. The distribution volumes of all tested polypeptide-DARPin fusion proteins were in the range of 1.95 to 2.57 mL (Table 2), indicating that they initially mainly distributed only in the intravascular space, from which extravasation to certain tissues as tumors may occur. This is corroborated by the shape of the bi-exponential decay curves of the serum concentration time curves, as the initial distribution phase is very short, followed by a long and steady elimination phase. All fusion proteins behaved similarly, with the exception of XTEN288-Ec1, which was characterized by a slightly longer lasting distribution phase and a larger decrease in the serum concentration during the first time points. Consequently, for this protein, the calculated AUC decreased and the V_d increased (Table 2), indicating faster equilibration and tissue distribution compared to the other polypeptide-DARPin fusion proteins (Fig. 2A).

3.1.5. Tumor uptake of PASylated and XTENylated DARPins correlates with serum half-life and molecular size

To further investigate the influence of charge and size on biodistribution in tumor-bearing mice, we conducted biodistribution and imaging studies. To this end, nude mice bearing EpCAM-positive HT29 tumor xenografts were injected i.v. with [^{99m}Tc](CO)$_3$ radiolabeled proteins. To quantify tumor uptake, 413 pmol protein labeled with 1 MBq were used and tumors were measured after 1, 4, 24 and 48 h. For SPECT imaging and tumor autoradiography, mice were injected i.v. with 532 pmol protein labeled with 7.5 MBq, and imaging was performed after 24 h prior to euthanasia and preparation of tumors for autoradiography to visualize intratumoral distribution.

As shown in Fig. 3A and Table S2, fusions with PAS and XTEN polypeptides greatly increased tumor uptake in a size-dependent manner, whereas systematic differences between the two polypeptide types of different charge were not detectable (Fig. 3A/Table S2). Twenty-four hours after injection, activity in the tumor reached 6.83 to 10.62%ID/g for the EpCAM-targeting fusion proteins. After 24 h, the tumor uptake of the unfused DARPin Ec1 was 2.05%ID/g for unmodified Ec1, and 0.56%ID/g for unmodified non-binding control DARPin Off7 (Fig. 3A/Table S2). Fusion proteins of the non-binding control fusions with DARPin Off7 also showed only a low uptake (1.00 to 5.01%ID/g) (Table S2), demonstrating only a small enhanced permeability and retention (EPR) effect.

To calculate a specificity index for tumor uptake of the fusion proteins, for each construct the uptake value of the EpCAM binder (Ec1 fusions) was divided by the one of the non-binder (Off7 fusions) (%ID/g tumor$_{binder}$/%ID/g tumor$_{non\text{-}binder}$), plotted over time (Fig. 3B). The time scales where tumor uptake is specific above levels of passive targeting (measured by Off7 fusions) differed among the constructs according to their size, but not according to the polypeptide charge. At early time points, differences between active and passive targeting were hardly detectable, whereas the effect of retention of the radiolabeled proteins by specific tumor cell binding increased with time. For all constructs, the specific uptake above levels of passive targeting became significant between 1 h and 4 h. This time was inversely correlated with molecular size, i.e., fusion with the shortest polypeptides increased specificity at earlier time points, while fusion with the longest polypeptides increased specificity at later time points.

Autoradiography of tumor slices visualized the spatial distribution of accumulated radiolabeled proteins within the tumor tissue. Tumor autoradiography 24 h after i.v. injection showed deep tissue penetration and distribution of the EpCAM-targeting polypeptide-DARPin fusion proteins (Fig. 3C). All constructs distributed equally well and largely independent of their size and charge. In contrast, the corresponding control fusion proteins with DARPin Off7 did not show any tissue distribution and penetration (Fig. 3C). On autoradiographs, activity of those control constructs was only detected in a thin vascularized layer in the periphery of the tumor. This underlines the high specificity of tumor uptake achieved with the targeting fusion proteins. Again, there was no detectable difference between the two polypeptide types. Tumor autoradiographs of unmodified DARPin Ec1 showed even distribution but very low activity, while the activity of control Off7 was essentially at background level. This demonstrates that fusions to PAS and XTEN to a binding protein effectively support specific active uptake and penetration in tumors, but do not lead to unspecific passive targeting.

3.1.6. PASylation and XTENylation of DARPins improves tumor uptake without increasing accumulation in non-target tissues

Biodistribution and imaging studies were conducted to test the effect of the intrinsically disordered polypeptide fusions, with and without negative charge, on unspecific accumulation in non-target tissues. To this end, mice bearing EpCAM-positive HT29 tumor xenografts were injected i.v. with [^{99m}Tc](CO)$_3$ radio-labeled proteins as described above. After 1, 4, 24 and 48 h tumor, blood, heart, lungs, stomach, intestine, kidneys, liver, spleen, bone and muscle were measured ex vivo for biodistribution of injected radiolabeled proteins. For SPECT imaging and tissue autoradiography, mice received a single i.v. injection as described above, and after 24 h they were SPECT-imaged prior to euthanasia and preparation of tissue slices of the right kidney and left liver lobe for tissue autoradiography and visualization of the local distribution of the injected proteins in sampled tissues.

Biodistribution (Fig. 4, Table S2) and SPECT imaging (Fig. 5, Fig. S4) show that fusion proteins of PAS and XTEN with Ec1 or the non-binding control DARPin Off7 did not accumulate in non-tumor tissues. In contrast to the tumor, only low activity levels were detected after 24 h. This therefore excludes off-target binding of the DARPins, unspecific interaction of the unstructured polypeptides with membrane components or other receptors or unspecific effects by the fusion proteins' charge or absence thereof. The longer half-life of the polypeptide-DARPin fusion proteins was reflected by the very gradually decreasing activity in the blood and in well-perfused organs like heart, lung and spleen (Fig. 4, Table S2). Furthermore, all other non-tumor tissues (Fig. 3A, Table S2) showed a trend in time-dependent decrease in

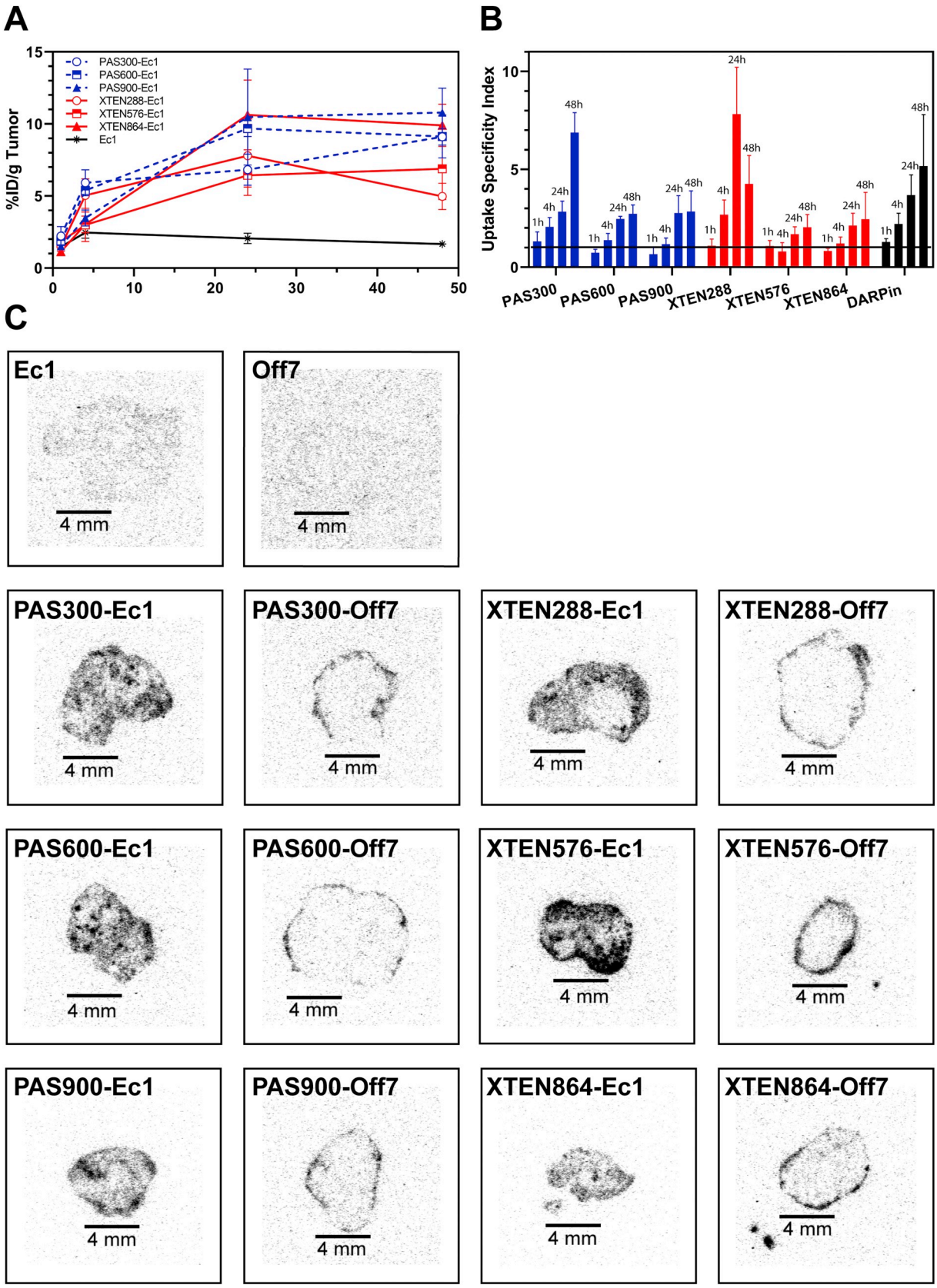

Fig. 3. Tumor uptake and tumor tissue distribution of radiolabeled PASylated and XTENylated EpCAM-binding DARPin Ec1 and control DARPin Off7 in mice bearing EpCAM-positive HT29 tumor xenografts. A) Tumor uptake (%ID/g tumor) of EpCAM targeting fusion proteins 1, 4, 24 and 48 h after i.v. injection of 412 pmol protein with 1 MBq specific activity of $[^{99m}Tc](CO)_3$. Data points are the averages of $N = 3$ mice ± SD. B) Uptake specificity 1, 4, 24, 48 h of the fusion proteins shown in (A). The specificity index was calculated by (%ID/g $tumor_{binder}$/%ID/g $tumor_{control}$). Data for control fusions are shown in Table S2. C) Autoradiographic images of 5 µm thick tumor slices. Tumors were frozen after excision from euthanized mice and cut into slices using a cryostat. Slices were placed on phosphor imaging plates overnight.

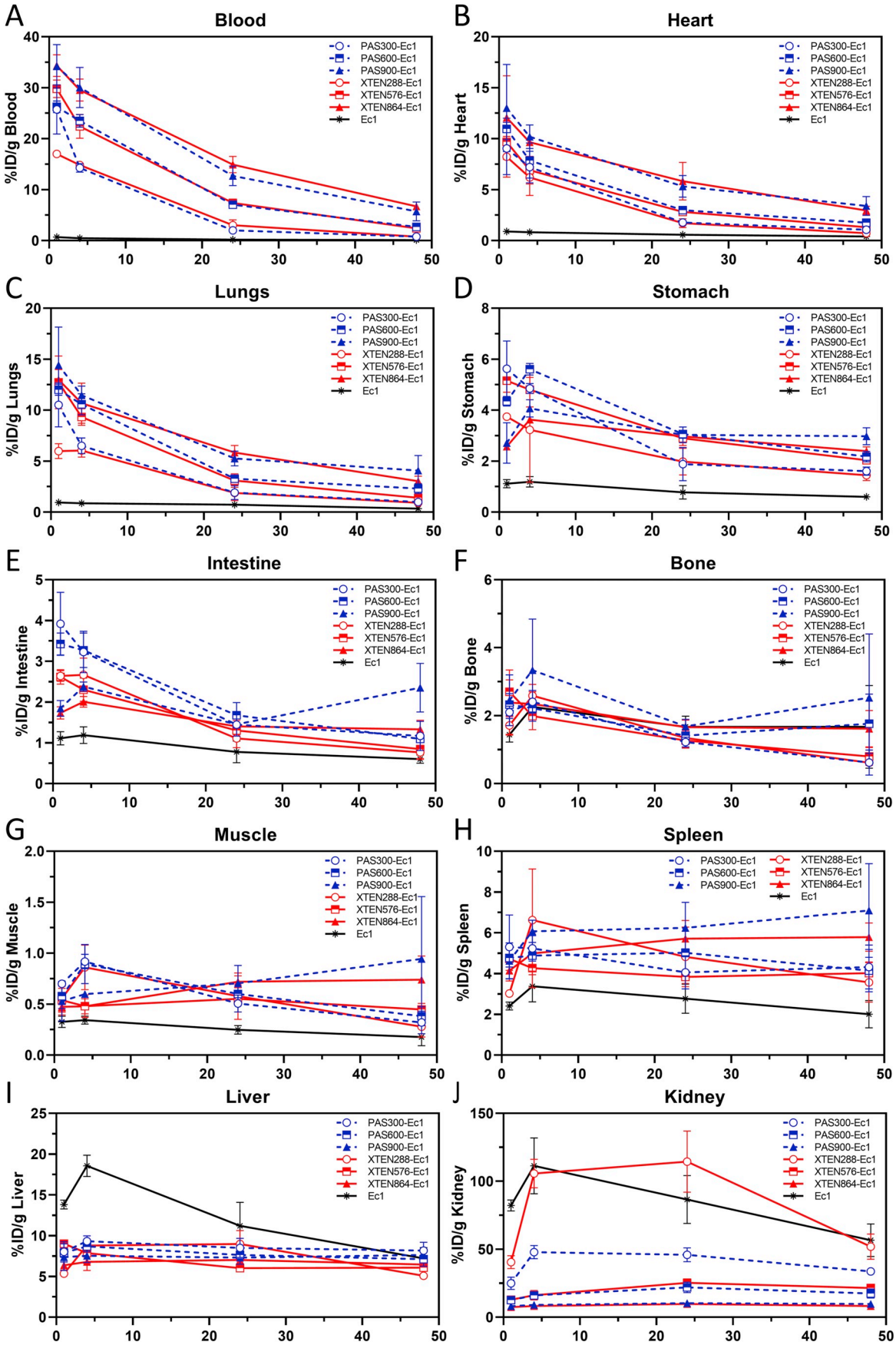

Fig. 4. Biodistribution of [^{99m}Tc](CO)$_3$ labeled PASylated and XTENylated DARPin Ec1 in mice bearing EpCAM-positive HT29 tumor xenografts. Mice (N = 3) were injected i.v. with 413 pmol protein containing 1 MBq specific activity. After 1, 4, 24 and 48 h, mice were euthanized and the activity (%ID/g tissue) in organs was measured with a γ-scintillation counter. Data points are average ± SD. The complete set of biodistribution data including all Off7 control constructs is shown in Table S2. A) Blood, B) Heart, C) Lungs, D) Stomach, E) Intestine, F) Bone, G) Muscle, H) Spleen, I) Kidney, J) Liver.

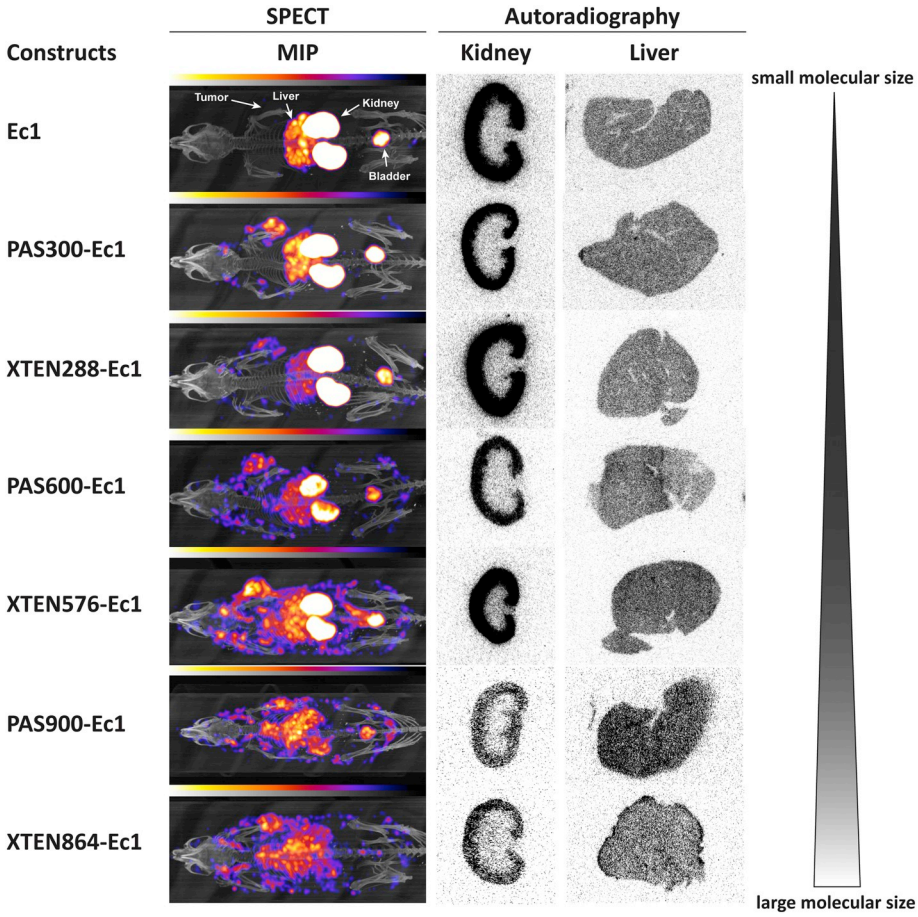

Fig. 5. Whole-body single-photon emission computer tomography (SPECT) imaging and tissue autoradiography of kidney and liver from mice bearing EpCAM-positive HT29 tumor xenografts. Mice were injected i.v. with 532 pmol [^{99m}Tc](CO)$_3$ -labeled polypeptide-DARPin Ec1 fusion protein or unmodified Ec1 with 7.5 MBq specific activity. Twenty-four hours after injection one mouse was anesthetized for SPECT imaging with isoflurane and imaged for 2 h. SPECT-images correspond to the maximum intensity projection (MIP). For kidney and liver autoradiography, organs were frozen in tissue-embedding solution ex vivo and cut into 5 µm thick slices using a cryostat. The slices were placed on phosphor imaging plates overnight and imaged using a phosphor plate reader.

activity, consistent with the time-dependent elimination of the radiolabeled proteins from the circulation, which was similar to that observed by sandwich ELISA (cf. Fig. 2A).

Kidney and liver as typical clearance organs were investigated for accumulation of the proteins. In the kidney, the decrease over time was in the same range for XTEN and PAS, when polypeptide-DARPin fusions of comparable length or hydrodynamic volume were compared. An inverse relationship of %ID/g and apparent molecular size could be observed: the larger the molecular size, the less activity in the kidney was measured, with most activities ranging from 45 to 7.5%ID/g kidney 24 h after injection (Fig. 4I/Table S2). Only XTEN288-Ec1 showed a higher trend to localize to the kidney, and was similar in this respect to the unfused DARPin Ec1. Interestingly, XTEN288-Ec1 had revealed a somewhat longer initial distribution phase and a higher apparent volume of distribution (Fig. 2A/Table 2) than the other fusion proteins, especially when compared to PAS300-Ec1, which is similar in size. Kidney autoradiography (Fig. 5) demonstrated for all proteins that activity was restricted to the renal cortex.

In the liver, radioactivity remained constant throughout the observed time period (Fig. 4J), with values for fusion proteins with DARPin Ec1 being slightly *lower* compared to those with control DARPin Off7 (Table S2). Liver activities of polypeptide-Ec1 fusion proteins ranged from 6.03 to 8.97%ID/g liver tissue after 24 h, without any correlation to molecular size, while polypeptide-Off7 fusions always showed *higher* liver activities, ranging from 6.15 to 15.79%ID/g liver. Control PAS-Off7 fusions showed the highest liver accumulations, decreasing with larger size, while XTEN-Off7 fusions showed lower activity and no obvious size-dependence (Table S2). SPECT imaging and autoradiography showed homogenous distribution in the liver tissue (Fig. 5/Fig. S4), without areas of deposits.

To better understand how the DARPin and the various polypeptide-DARPin fusion proteins are eliminated from the body, urine and feces were collected 24 h after injection. In the urine, low levels of activity ranging from 0.5 to 1.6% of the injected dose were measured and no trend was observed with respect to molecular weight, mass, or whether the targeting DARPin or the control DARPin was considered (Table S3, Fig. S5). This finding was corroborated by kidney autoradiography and SPECT imaging (Fig. 5/Fig. S4). Only traces of activity were detected in the feces (0.24 to 0.78%ID) (Table S3), again with no trend regarding mass, charge or DARPin identity.

4. Discussion

Naturally occurring intrinsically disordered proteins (IDPs) have been recognized as an integral part of cellular function [50,51] and evolution has optimized them for solubility and resistance to proteases, but usually targeted them to be at the brink of folding and binding, or involved in association with other partners to result in a phase separation phenomenon [50,52,53]. Similarly, synthetic unstructured proteins, as the PAS and XTEN polypeptides used here [21,22], also avoid hydrophobic residues, but are either completely uncharged (PAS), or carry only negative charges (XTEN), since polycations would be problematic for drug delivery [54]. In both cases of PAS and XTEN, sequence patterns are avoided that would be commensurate with secondary structure formation.

Therefore, these synthetic IDPs do not appear to fold, associate or aggregate, and behave as monomers with a very large hydrodynamic radius of a random-flight polymer, somewhat larger for the negatively charged ones because of internal repulsions. This makes them highly suitable for fusions to therapeutic proteins, in a conceptually similar manner as conjugation with PEG [5,55–57]. The hydrodynamic radii of PAS300 and XTEN288 fusion proteins, as determined by the sizes from

analytical SEC, were in the range of proteins conjugated with PEG polymers of a nominal molecular weight of 20 kDa [58]. The polypeptides of longer chain length would be similar to the largest PEGs available for conjugation [40].

The production and purification of proteins with such properties can be a challenge, compounded by potential recombination of repetitive protein sequences, inaccessibility of tags, impurities directly bound to the unstructured region and their unusual behavior on ion exchange columns. Incomplete polypeptide-DARPin fusion proteins, resulting from either incomplete translation or degradation are not well detectable by Coomassie-stained protein gels, because they do not contain basic or hydrophobic amino acids to which the stain predominantly binds, and such side products are thus only detectable at the end by peptide bond absorption at 210 nm [59]. Despite these initial difficulties, we established a very robust high-yielding lab scale procedure which is independent of the polypeptide size and works equally well for the charged XTEN and uncharged PAS polypeptides, and is independent of the properties of the DARPin or other protein of interest. A *rec*A-deficient *E. coli* strain was used for cytoplasmic expression to prevent possible recombination of the repetitive polypeptide sequences containing tandem repeats. To eliminate potentially incompletely synthesized polypeptides, we employ affinity tags at both ends, first using the C-terminal His-tag, followed by capturing the N-terminal sfGFP tag with an anti-GFP-affinity column [45], which permits rigorous washing and subsequent proteolytic elution. A final polishing step by preparative gel filtration leads to the desired products (Fig. 1). In summary, this three-step purification strategy yielded protein preparations of extraordinary purity without co-purified *E. coli* impurities and entirely devoid of incompletely translated polypeptide-DARPin species as shown by SDS-PAGE (Fig. 1B), Western blots (Fig. S1), and ESI-MS (Fig. S2, Table 1).

Incubation of DARPins [37], and of PAS [21] and XTEN [22] polypeptides with mouse serum showed no signs of degradation, whereas incubation with kidney homogenate showed rapid degradation of all proteins. This finding and the long terminal half-lives of more than 20 h of the longest polypeptides are consistent with the fact that the polypeptide-DARPin fusion proteins are resistant to proteolytic degradation in serum. However, we could detect low levels of small hydrophilic $[^{99m}Tc](CO)_3$ metabolites (Fig. S5) in the urine, suggesting that small amounts of the label are cleaved from the proteins and then directly eliminated through the kidney. Due to the residualizing property of $[^{99m}Tc](CO)_3$ in cells this must occur in the extracellular space.

When fusing or conjugating a large, flexible polymer to a binding protein, even when doing so remotely from the paratope, a transient blocking will result [48] that manifests itself in a slightly reduced association rate constant (k_a), but an identical dissociation rate constant (k_d), the latter indicating an unchanged binding site. What has been established before with PEG-conjugated antibody scFv fragments [48] was also observed here with PAS and XTEN fusions to DARPin Ec1. We observed a modest decrease (2–3 fold) of k_a, while k_d remained essentially unchanged. Therefore, the apparent equilibrium dissociation constant (K_D) increased by the same small factor, however, this small decrease in affinity is negligible since it is still in the picomolar range. Within the accuracy of the measurements, no clear trend of polymer size or charge was discernable for the kinetic parameters, and we cannot rule out a potentially very small influence of the negatively charged alginate chip surface on the XTEN fusions, which would have to be studied further.

In a side-by-side comparison of sets of fusion proteins of PAS and XTEN with 300 and 288 aa, 600 and 576 aa, as well as 900 and 864 aa, respectively, we found that the serum half-life can be correlated across both types of proteins very well to the hydrodynamic radius, as measured by elution volume on analytical SEC (Fig. 2B). It might have been expected a priori that XTEN, due to its high negative charge and the electrostatic repulsion from membranes, would show a stronger half-life extension effects than PAS, but this was not observed, when taking the hydrodynamic radius into account.

For all constructs, except XTEN288-Ec1, distribution phase (α-phase) and elimination phase (β-phase) can hardly be distinguished after i.v. injection and the apparent volume of distribution (V_d) was in the range of the serum volume of mice. This suggests that the injected proteins were largely restricted to the intravascular space from which also elimination occurs. XTEN288-Ec1 differs with its more pronounced and rapid distribution and elimination and a larger apparent volume of distribution (V_d), indicating that this specific construct better equilibrates with tissues. Consequently, the faster elimination kinetics of XTEN288-Ec1 correlated with a stronger labeling of the kidneys, similar to the unfused DARPin. This observation may help to choose the construct with the optimal pharmacokinetics, depending on the desired application.

The pharmacokinetic data observed here, using the same DARPin fusion on both systems, are similar to those that have been reported with other fusions to proteins of interest, e.g. to IFN, Fab fragments or peptides (often only one fusion protein was reported) [21,23]; small differences are most likely due to the influence of the fused payload, as well as unavoidable differences in the detection method, dosing and observation time points. Nevertheless, it appears that, in a first approximation, the properties of the fusion protein are given by the hydrodynamic properties of the intrinsically disordered protein fused to the protein of interest.

The efficiency of tumor uptake as a function of affinity and size has been studied before both in simulations based on literature data [60,61] as well as by direct experimental measurements [40]. Both lines of evidence agree that efficient tumor uptake can be achieved with very small binding proteins having very high affinity or, more efficiently, with much larger targeting proteins with long serum half-lives, but not so well with proteins of intermediate molecular weights [40,60,61]. In the present study, only one very small protein and a systematic set of rather large proteins were compared, and we observed a correlated increase between molecular size and tumor accumulation. All constructs were monomeric and had very similar picomolar affinity, and our data match well with the data in the simulations [60,61]. The proteins with larger size accumulated in the tumors with slower kinetics than their smaller counterparts. This could result from a combination of reduced extravasation rates, and smaller diffusion coefficients of larger molecules, amplified by crowding effects on the molecular level.

Because of the increased serum persistence and lower clearance of larger molecules, at any given time the blood acts as a reservoir for extravasation, and thus with higher serum concentrations higher tissue accumulation can be expected. This was also observed for the non-binding control fusion proteins, although at a very low level. The low tumor accumulation of the control constructs suggests only a marginal role of passive tumor targeting by the enhanced permeability and retention (EPR) effect [62]. A further increase of the size, however, may not necessarily result in even higher uptake due to a substantial drop in the vascular extravasation rate with increasing molecular size [63]. In fact, as shown by simulations, tumor uptake continually *decreases* as size increases above 20 nm in radius.

Our tumor autoradiography data show good tumor penetration and essentially a homogeneous distribution within the HT29 tumor tissue for targeted polypeptide-DARPin fusions — if only a subset of cells were reached in treatments, drug resistance would inevitably emerge. In contrast, localization of the non-targeted control fusions was restricted to a thin vascularized layer in the tumor periphery, which was most likely due to molecules remaining in the blood pool. Altogether, in tumor uptake and tissue distribution experiments we could again not find a difference between PASylation and XTENylation. On the other hand, we cannot rigorously exclude yet that possible electrostatic repulsion of the XTEN polypeptides by cellular membranes might impede *cellular* uptake and might thus limit the anti-tumor effect of certain cytotoxic conjugates, and this requires further investigations.

It has been well known that antibodies typically show high tumor uptake, but very limited penetration and distribution within tumors

[64,65]. Early proposals that this is entirely due to steric hindrance have been largely refuted, and instead today this is usually explained by a combination of high affinity saturation of binding sites at a given dose, proceeding from the tumor outside to inside [61,66,67], often with subsequent receptor internalization after bivalent binding. Even though the affinity of the DARPin used here is picomolar, it is possible that their monovalency is a factor in the observed excellent tumor penetration.

The proteins with the longest half-lives are those that use FcRn recycling, namely IgG and serum albumin. In mice, the half-life of mouse albumin is about 30 h, while in the absence of FcRn recycling, it is about 20 h [68,69], which is also the range of non-FcRn recycled IgGs [70,71]. Fusions of the largest polypeptides (PAS900 and XTEN864) are in this range (Table 2). Thus, the PAS900 and XTEN864 fusions to DARPin Ec1 increased the half-life in mice similarly as conjugation with human serum albumin [37], which also does not show FcRn recycling in w.t. mice (Merten et al., manuscript in preparation). It is currently unclear whether significantly longer half-lives than observed here can be reached in the absence of FcRn recycling, and in occasional reports of longer half-lives in mice, the accuracy of the measurements needs to be critically examined. Allometric scaling as well as some clinical testing suggests that the longest PAS and XTEN polypeptides may approach serum half-lives of up to 10 days in man [23].

An important difference to be further explored is that the XTEN and PAS fusions, with the exception of XTEN288-Ec1, were mainly confined to the intravascular compartment, unlike albumin and albumin fusions, which are also found in interstitial spaces. Additionally, the FcRn recycling within endothelial cells, which does not occur for the fusions tested here, can alter the type of off-target exposure between such half-life extended molecules. Furthermore, the differences in extravasation between a compact globular protein such as serum albumin and the fusions examined here, formally of larger size but much more flexible, has not yet been explored.

Although differences in target properties, expression levels, and differences in radiolabeling make the comparison of different tumor accumulation studies intrinsically difficult, similar levels were found here as in related studies. Intratumoral accumulation of PASylated and XTENylated DARPin Ec1 is comparable to a PEGylated Her2-binding DARPin [40]. Compared to a Fab-PAS600 fusion protein [72], the PAS600-DARPin fusion proteins lead to an almost 50% higher uptake. Fab-ABD fusions tested in the same study showed similar high tumor uptake rates as the largest PAS-/XTEN-DARPin fusions of the present study. In aggregate, these studies show that PASylation and XTENylation can achieve similar tumor accumulation levels in mice as FcRn-recycled fusion proteins.

The biodistribution studies with the radiolabeled PASylated and XTENylated DARPin fusion proteins and of unmodified DARPins showed no non-specific accumulation in non-tumor tissues after i.v. injection. The levels measured in all organs were background; the detectable levels followed the blood elimination kinetics and simply indicated the gradual elimination from the circulation. This confirms that neither the fused nor the unfused DARPins accumulated in tissues not expressing EpCAM, and that the PAS and XTEN fusions did not cause any non-specific accumulation by themselves, consistent with previous reports [23,59,72], as well as reports on PEGylated DARPins [40].

Due to their role in metabolism and clearance, the liver and the kidneys are the most critical organs affected by therapies involving cytotoxic proteins, and dose-limiting adverse effects often have their origins at these organs. It is thus important to study the clearance mechanism of these IDP-fusion proteins. We found that the liver showed rather constant but modest levels of radiolabeled polypeptide-DARPin fusion proteins throughout the experiments, independent of size and charge. This is in line with other non-accumulating half-life extended molecules [40,58,59,72–75] and suggests that the liver is not a major site for metabolism and elimination of such molecules [23].

In contrast, the kidney was the major organ of clearance for all tested fusion protein constructs. We observed a size-dependent accumulation of radioactivity and, within the 48 h of measurement, polypeptide-DARPin fusions with larger size always showed lower levels detected in biodistribution experiments as well as by kidney autoradiography and SPECT imaging. $[^{99m}Tc](CO)_3$ is a residualizing label, which remains trapped in cells after endocytosis and degradation of the proteins, as there is no retrograde transporter. It thus reflects the total amount of radiolabeled protein which has entered this compartment until the time of measurement. This amount is smaller for the larger proteins because, as shown in Fig. 2, their elimination is delayed and a substantial amount still remains in the circulation 48 h after injection. The residualizing property of $[^{99m}Tc](CO)_3$ also suggests that the low levels of free label in the urine detected by autoradiography of SDS-PAGE gels (Fig. S5) result from extracellular cleavage somewhere in the body. The lack of full-length polypeptide-DARPin fusions in the urine can be expected from an intact kidney function.

Our autoradiography data of the renal cortex do not discriminate between radioactivity in cells of the glomerulus or the proximal tubule. Nevertheless, one can expect that the smaller proteins pass the glomerular filter and end up in the tubular epithelial cells, whereas the larger ones are retained and may be degraded in the glomerulus. Recent evidence indeed suggests that degradation of proteins in the kidney can occur at two sites, the proximal tubule and the glomerulus, where the required transport systems are expressed in podocytes, which in addition express a plethora of intracellular and extracellular proteases [76,77]. On the other hand, this does not explain uptake of the negatively charged XTEN polypeptides, which accumulated in the renal cortex similarly as the uncharged PAS proteins of the same size, even though one might have expected a repulsion by negatively charged structures in the glomerular basement membrane [77]. For these charged proteins the renal mesangial space is the only site where accumulation can occur [78,79], as it is directly accessible through the glomerular vascular fenestrations, which typically have a relatively wide width of 70 to 130 nm. From here, internalization and degradation of the proteins by macrophages and mesangial cells may occur [80].

A major fraction of peptides and small proteins developed for tumor targeting is cleared rapidly from the circulation before efficient tumor uptake and hence before anti-tumor effects are achieved. The use of PAS and XTEN polypeptides of different length fused to the same DARPin, produced and purified in a robust method, allowed us to systematically investigate the role of the size and charge for serum half-life, biodistribution and tumor uptake in mice without any other variations. Pharmacokinetic analyses showed a clear linear relationship between hydrodynamic radius of the unstructured polypeptide, half-life and AUC, across both polypeptide types and independent of charge. Most importantly, extended serum half-life of the fusion proteins consistently increased tumor uptake without increasing unspecific accumulation in non-target tissues including liver and kidneys, and we found the kidney to be the major site of excretion for all constructs. In summary, we conclude that the ability to precisely engineer the half-life of therapeutic proteins by design using unstructured polypeptides holds great promise in increasing the options for effective tumor targeting.

Acknowledgements

The authors would like to thank Dr. Henrik Braband for advice in radiolabeling of proteins, and Saskia Jakob and Stefan Imobersteg for their valuable and enduring support in realizing the biodistribution and imaging studies. This work was supported by the Schweizerische Nationalfonds [grant number 31003A-170134].

Appendix A. Supplementary data

Supplementary data to this article can be found online at https://doi.org/10.1016/j.jconrel.2019.06.030.

References

[1] U.H. Weidle, J. Auer, U. Brinkmann, G. Georges, G. Tiefenthaler, The emerging role of new protein scaffold-based agents for treatment of cancer, Cancer Genomics Proteomics, 10 (2013) 155–168.
[2] K. Skrlec, B. Strukelj, A. Berlec, Non-immunoglobulin scaffolds: a focus on their targets, Trends Biotechnol., 33 (2015) 408–418.
[3] R. Vazquez-Lombardi, T.G. Phan, C. Zimmermann, D. Lowe, L. Jermutus, D. Christ, Challenges and opportunities for non-antibody scaffold drugs, Drug Discov. Today 20 (2015) 1271–1283.
[4] B. Owens, Faster, deeper, smaller - the rise of antibody-like scaffolds, Nat. Biotechnol. 35 (2017) 602–603.
[5] G. Pasut, F.M. Veronese, State of the art in PEGylation: the great versatility achieved after forty years of research, J. Control. Release 161 (2012) 461–472.
[6] J.I. Lee, S.P. Eisenberg, M.S. Rosendahl, E.A. Chlipala, J.D. Brown, D.H. Doherty, G.N. Cox, Site-specific PEGylation enhances the pharmacokinetic properties and antitumor activity of interferon beta-1b, J. Interf. Cytokine Res. 33 (2013) 769–777.
[7] D. Bagal, H. Zhang, P.D. Schnier, Gas-phase proton-transfer chemistry coupled with TOF mass spectrometry and ion mobility-MS for the facile analysis of poly(ethylene glycols) and PEGylated polypeptide conjugates, Anal. Chem. 80 (2008) 2408–2418.
[8] R.R. Abzalimov, A.K. Frimpong, I.A. Kaltashov, Detection and characterization of large-scale protein conformational transitions in solution using charge-state distribution analysis in ESI-MS, Methods Mol. Biol., 896 (2012) 365–373.
[9] J.K. Dozier, M.D. Distefano, Site-specific PEGylation of therapeutic proteins, Int. J. Mol. Sci. 16 (2015) 25831–25864.
[10] D.G. Rudmann, J.T. Alston, J.C. Hanson, S. Heidel, High molecular weight polyethylene glycol cellular distribution and PEG-associated cytoplasmic vacuolation is molecular weight dependent and does not require conjugation to proteins, Toxicol. Pathol. 41 (2013) 970–983.
[11] I.A. Ivens, W. Achanzar, A. Baumann, A. Brandli-Baiocco, J. Cavagnaro, M. Dempster, B.O. Depelchin, A.R. Rovira, L. Dill-Morton, J.H. Lane, B.M. Reipert, T. Salcedo, B. Schweighardt, L.S. Tsuruda, P.L. Turecek, J. Sims, PEGylated biopharmaceuticals: current experience and considerations for nonclinical development, Toxicol. Pathol. 43 (2015) 959–983.
[12] P. Zhang, F. Sun, S. Liu, S. Jiang, Anti-PEG antibodies in the clinic: current issues and beyond PEGylation, J. Control. Release 244 (2016) 184–193.
[13] J.K. Armstrong, G. Hempel, S. Koling, L.S. Chan, T. Fisher, H.J. Meiselman, G. Garratty, Antibody against poly(ethylene glycol) adversely affects PEG-asparaginase therapy in acute lymphoblastic leukemia patients, Cancer 110 (2007) 103–111.
[14] C. Cantante, S. Lourenco, M. Morais, J. Leandro, L. Gano, N. Silva, P. Leandro, M. Serrano, A.O. Henriques, A. Andre, C. Cunha-Santos, C. Fontes, J.D.G. Correia, F. Aires-da-Silva, J. Goncalves, Albumin-binding domain from Streptococcus zooepidemicus protein Zag as a novel strategy to improve the half-life of therapeutic proteins, J. Biotechnol. 253 (2017) 23–33.
[15] D. Steiner, F.W. Merz, I. Sonderegger, M. Gulotti-Georgieva, D. Villemagne, D.J. Phillips, P. Forrer, M.T. Stumpp, C. Zitt, H.K. Binz, Half-life extension using serum albumin-binding DARPin® domains, Protein Eng. Des. Sel. 30 (2017) 583–591.
[16] F. Unverdorben, F. Richter, M. Hutt, O. Seifert, P. Malinge, N. Fischer, R.E. Kontermann, Pharmacokinetic properties of IgG and various Fc fusion proteins in mice, mAbs 8 (2016) 120–128.
[17] R.E. Kontermann, Half-life extended biotherapeutics, Expert. Opin. Biol. Ther. 16 (2016) 903–915.
[18] W.R. Strohl, Fusion proteins for half-life extension of biologics as a strategy to make biobetters, Biodrugs 29 (2015) 215–239.
[19] M. Bern, K.M. Sand, J. Nilsen, I. Sandlie, J.T. Andersen, The role of albumin receptors in regulation of albumin homeostasis: implications for drug delivery, J. Control. Release 211 (2015) 144–162.
[20] C.L. Anderson, J. Kim, Surmounting an impasse of FcRn structure, Structure 21 (2013) 1907–1908.
[21] M. Schlapschy, U. Binder, C. Borger, I. Theobald, K. Wachinger, S. Kisling, D. Haller, A. Skerra, PASylation: a biological alternative to PEGylation for extending the plasma half-life of pharmaceutically active proteins, Protein Eng. Des. Sel. 26 (2013) 489–501.
[22] V. Schellenberger, C.W. Wang, N.C. Geething, B.J. Spink, A. Campbell, W. To, M.D. Scholle, Y. Yin, Y. Yao, O. Bogin, J.L. Cleland, J. Silverman, W.P. Stemmer, A recombinant polypeptide extends the in vivo half-life of peptides and proteins in a tunable manner, Nat. Biotechnol. 27 (2009) 1186–1190.
[23] V.N. Podust, S. Balan, B.C. Sim, M.P. Coyle, U. Ernst, R.T. Peters, V. Schellenberger, Extension of in vivo half-life of biologically active molecules by XTEN protein polymers, J. Control. Release 240 (2016) 52–66.
[24] M. Gebauer, A. Skerra, Prospects of PASylation® for the design of protein and peptide therapeutics with extended half-life and enhanced action, Bioorg. Med. Chem. 26 (2018) 2882–2887.
[25] M. Simon, N. Stefan, A. Plückthun, U. Zangemeister-Wittke, Epithelial cell adhesion molecule-targeted drug delivery for cancer therapy, Expert Opin. Drug Deliv. 10 (2013) 451–468.
[26] C. Patriarca, R.M. Macchi, A.K. Marschner, H. Mellstedt, Epithelial cell adhesion molecule expression (CD326) in cancer: a short review, Cancer Treat. Rev. 38 (2012) 68–75.
[27] A. Plückthun, Designed ankyrin repeat proteins (DARPins): binding proteins for research, diagnostics, and therapy, Annu. Rev. Pharmacol. Toxicol. 55 (2015) 489–511.
[28] H.K. Binz, M.T. Stumpp, P. Forrer, P. Amstutz, A. Plückthun, Designing repeat proteins: well-expressed, soluble and stable proteins from combinatorial libraries of consensus ankyrin repeat proteins, J. Mol. Biol. 332 (2003) 489–503.
[29] H.K. Binz, P. Amstutz, A. Kohl, M.T. Stumpp, C. Briand, P. Forrer, M.G. Grütter, A. Plückthun, High-affinity binders selected from designed ankyrin repeat protein libraries, Nat. Biotechnol. 22 (2004) 575–582.
[30] D. Steiner, P. Forrer, A. Plückthun, Efficient selection of DARPins with sub-nanomolar affinities using SRP phage display, J. Mol. Biol. 382 (2008) 1211–1227.
[31] G. Interlandi, S.K. Wetzel, G. Settanni, A. Plückthun, A. Caflisch, Characterization and further stabilization of designed ankyrin repeat proteins by combining molecular dynamics simulations and experiments, J. Mol. Biol. 375 (2008) 837–854.
[32] C. Zahnd, F. Pecorari, N. Straumann, E. Wyler, A. Plückthun, Selection and characterization of Her2 binding-designed ankyrin repeat proteins, J. Biol. Chem. 281 (2006) 35167–35175.
[33] N. Stefan, P. Martin-Killias, S. Wyss-Stoeckle, A. Honegger, U. Zangemeister-Wittke, A. Plückthun, DARPins recognizing the tumor-associated antigen EpCAM selected by phage and ribosome display and engineered for multivalency, J. Mol. Biol. 413 (2011) 826–843.
[34] T. Tsaktanis, H. Kremling, M. Pavsic, R. von Stackelberg, B. Mack, A. Fukumori, H. Steiner, F. Vielmuth, V. Spindler, Z. Huang, J. Jakubowski, N.H. Stoecklein, E. Luxenburger, K. Lauber, B. Lenarcic, O. Gires, Cleavage and cell adhesion properties of human epithelial cell adhesion molecule (HEPCAM), J. Biol. Chem. 291 (2016) 425.
[35] N. Stefan, M. Zimmermann, M. Simon, U. Zangemeister-Wittke, A. Plückthun, Novel prodrug-like fusion toxin with protease-sensitive bioorthogonal PEGylation for tumor targeting, Bioconjug. Chem. 25 (2014) 2144–2156.
[36] M. Simon, N. Stefan, L. Borsig, A. Plückthun, U. Zangemeister-Wittke, Increasing the antitumor effect of an EpCAM-targeting fusion toxin by facile click PEGylation, Mol. Cancer Ther. 13 (2014) 375–385.
[37] M. Simon, R. Frey, U. Zangemeister-Wittke, A. Plückthun, Orthogonal assembly of a designed ankyrin repeat protein-cytotoxin conjugate with a clickable serum albumin module for half-life extension, Bioconjug. Chem. 24 (2013) 1955–1966.
[38] M. Simon, U. Zangemeister-Wittke, A. Plückthun, Facile double-functionalization of designed ankyrin repeat proteins using click and thiol chemistries, Bioconjug. Chem. 23 (2012) 279–286.
[39] P. Martin-Killias, N. Stefan, S. Rothschild, A. Plückthun, U. Zangemeister-Wittke, A novel fusion toxin derived from an EpCAM-specific designed ankyrin repeat protein has potent antitumor activity, Clin. Cancer Res. 17 (2011) 100–110.
[40] C. Zahnd, M. Kawe, M.T. Stumpp, C. de Pasquale, R. Tamaskovic, G. Nagy-Davidescu, B. Dreier, R. Schibli, H.K. Binz, R. Waibel, A. Plückthun, Efficient tumor targeting with high-affinity designed ankyrin repeat proteins: effects of affinity and molecular size, Cancer Res. 70 (2010) 1595–1605.
[41] F. Andres, L. Iamele, T. Meyer, J.C. Stüber, F. Kast, E. Gherardi, H.H. Niemann, A. Plückthun, Inhibition of the MET kinase activity and cell growth in MET-addicted cancer cells by bi-paratopic linking, J. Mol. Biol. 431 (2019) 2020–2039.
[42] J.D. Pedelacq, S. Cabantous, T. Tran, T.C. Terwilliger, G.S. Waldo, Engineering and characterization of a superfolder green fluorescent protein, Nat. Biotechnol. 24 (2006) 79–88.
[43] H.K. Binz, P. Amstutz, A. Kohl, M.T. Stumpp, C. Briand, P. Forrer, M.G. Grütter, A. Plückthun, High-affinity binders selected from designed ankyrin repeat protein libraries, Nat. Biotechnol. 22 (2004) 575–582.
[44] F.W. Studier, Stable expression clones and auto-induction for protein production in E. coli, Methods Mol. Biol. 1091 (2014) 17–32.
[45] S. Hansen, J.C. Stüber, P. Ernst, A. Koch, D. Bojar, A. Batyuk, A. Plückthun, Design and applications of a clamp for green fluorescent protein with picomolar affinity, Sci. Rep. 7 (2017) 16292.
[46] R. Waibel, R. Alberto, J. Willuda, R. Finnern, R. Schibli, A. Stichelberger, A. Egli, U. Abram, J.P. Mach, A. Plückthun, P.A. Schubiger, Stable one-step technetium-99m labeling of his-tagged recombinant proteins with a novel Tc(I)-carbonyl complex, Nat. Biotechnol. 17 (1999) 897–901.
[47] P. Goffin, P. Dehottay, Complete genome sequence of Escherichia coli BLR(DE3), a recA-deficient derivative of E. coli BL21(DE3), Genome Announc 5 (2017) e00441–17.
[48] S. Kubetzko, C.A. Sarkar, A. Plückthun, Protein PEGylation decreases observed target association rates via a dual blocking mechanism, Mol. Pharmacol. 68 (2005) 1439–1454.
[49] M.E. Chapman, L. Hu, C.F. Plato, D.E. Kohan, Bioimpedance spectroscopy for the estimation of body fluid volumes in mice, Am. J. Physiol. Renal Physiol. 299 (2010) F280–F283.
[50] V.N. Uversky, Intrinsically disordered proteins in overcrowded milieu: membraneless organelles, phase separation, and intrinsic disorder, Curr. Opin. Struct. Biol. 44 (2017) 18–30.
[51] V.N. Uversky, Dancing protein clouds: the strange biology and chaotic physics of intrinsically disordered proteins, J. Biol. Chem. 291 (2016) 6681–6688.
[52] A.V. Fonin, A.L. Darling, I.M. Kuznetsova, K.K. Turoverov, V.N. Uversky, Intrinsically disordered proteins in crowded milieu: when chaos prevails within the cellular gumbo, Cell. Mol. Life Sci. 75 (2018) 3907–3929.
[53] V.N. Uversky, Protein intrinsic disorder-based liquid-liquid phase transitions in biological systems: complex coacervates and membrane-less organelles, Adv. Colloid Interf. Sci. 239 (2017) 97–114.
[54] A. Bernkop-Schnürch, Strategies to overcome the polycation dilemma in drug delivery, Adv. Drug Deliv. Rev. 136-137 (2018) 62–72.
[55] R.B. Greenwald, Y.H. Choe, J. McGuire, C.D. Conover, Effective drug delivery by PEGylated drug conjugates, Adv. Drug Deliv. Rev. 55 (2003) 217–250.
[56] J.M. Harris, R.B. Chess, Effect of PEGylation on pharmaceuticals, Nat. Rev. Drug Discov. 2 (2003) 214–221.
[57] S.A. Marshall, G.A. Lazar, A.J. Chirino, J.R. Desjarlais, Rational design and

engineering of therapeutic proteins, Drug Discov. Today 8 (2003) 212–221.
[58] S. Kubetzko, E. Balic, R. Waibel, U. Zangemeister-Wittke, A. Plückthun, PEGylation and multimerization of the anti-p185HER-2 single chain Fv fragment 4D5: effects on tumor targeting, J. Biol. Chem. 281 (2006) 35186–35201.
[59] A. Haeckel, F. Appler, L. Figge, H. Kratz, M. Lukas, R. Michel, J. Schnorr, M. Zille, B. Hamm, E. Schellenberger, XTEN-annexin A5: XTEN allows complete expression of long-circulating protein-based imaging probes as recombinant alternative to PEGylation, J. Nucl. Med. 55 (2014) 508–514.
[60] M.M. Schmidt, K.D. Wittrup, A modeling analysis of the effects of molecular size and binding affinity on tumor targeting, Mol. Cancer Ther. 8 (2009) 2861–2871.
[61] K.D. Wittrup, G.M. Thurber, M.M. Schmidt, J.J. Rhoden, Practical theoretic guidance for the design of tumor-targeting agents, Methods Enzymol. 503 (2012) 255–268.
[62] K. Greish, Enhanced permeability and retention of macromolecular drugs in solid tumors: a royal gate for targeted anticancer nanomedicines, J. Drug Target. 15 (2007) 457–464.
[63] M.R. Dreher, W. Liu, C.R. Michelich, M.W. Dewhirst, F. Yuan, A. Chilkoti, Tumor vascular permeability, accumulation, and penetration of macromolecular drug carriers, J. Natl. Cancer Inst. 98 (2006) 335–344.
[64] R. Sutherland, F. Buchegger, M. Schreyer, A. Vacca, J.P. Mach, Penetration and binding of radiolabeled anti-carcinoembryonic antigen monoclonal antibodies and their antigen binding fragments in human colon multicellular tumor spheroids, Cancer Res. 47 (1987) 1627–1633.
[65] R. Muchekehu, D. Liu, M. Horn, L. Campbell, J. Del Rosario, M. Bacica, H. Moskowitz, T. Osothprarop, A. Dirksen, V. Doppalapudi, A. Kaspar, S.R. Pirie-Shepherd, J. Coronella, The effect of molecular weight, PK, and valency on tumor biodistribution and efficacy of antibody-based drugs, Transl. Oncol. 6 (2013) 562–572.
[66] G.M. Thurber, M.M. Schmidt, K.D. Wittrup, Antibody tumor penetration: transport opposed by systemic and antigen-mediated clearance, Adv. Drug Deliv. Rev. 60 (2008) 1421–1434.
[67] G.M. Thurber, K. Dane Wittrup, A mechanistic compartmental model for total antibody uptake in tumors, J. Theor. Biol. 314 (2012) 57–68.
[68] C. Chaudhury, S. Mehnaz, J.M. Robinson, W.L. Hayton, D.K. Pearl, D.C. Roopenian, C.L. Anderson, The major histocompatibility complex-related Fc receptor for IgG (FcRn) binds albumin and prolongs its lifespan, J. Exp. Med. 197 (2003) 315–322.
[69] J.T. Andersen, B. Dalhus, D. Viuff, B.T. Ravn, K.S. Gunnarsen, A. Plumridge, K. Bunting, F. Antunes, R. Williamson, S. Athwal, E. Allan, L. Evans, M. Bjoras, S. Kjaerulff, D. Sleep, I. Sandlie, J. Cameron, Extending serum half-life of albumin by engineering neonatal Fc receptor (FcRn) binding, J. Biol. Chem. 289 (2014) 13492–13502.
[70] V. Ghetie, J.G. Hubbard, J.K. Kim, M.F. Tsen, Y. Lee, E.S. Ward, Abnormally short serum half-lives of IgG in beta 2-microglobulin-deficient mice, Eur. J. Immunol. 26 (1996) 690–696.
[71] E.J. Israel, D.F. Wilsker, K.C. Hayes, D. Schoenfeld, N.E. Simister, Increased clearance of IgG in mice that lack beta 2-microglobulin: possible protective role of FcRn, Immunology 89 (1996) 573–578.
[72] C.T. Mendler, L. Friedrich, I. Laitinen, M. Schlapschy, M. Schwaiger, H.J. Wester, A. Skerra, High contrast tumor imaging with radio-labeled antibody Fab fragments tailored for optimized pharmacokinetics via PASylation, mAbs 7 (2015) 96–109.
[73] V.N. Podust, B.C. Sim, D. Kothari, L. Henthorn, C. Gu, C.W. Wang, B. McLaughlin, V. Schellenberger, Extension of in vivo half-life of biologically active peptides via chemical conjugation to XTEN protein polymer, Protein Eng. Des. Sel. 26 (2013) 743–753.
[74] M. Altai, H. Liu, H. Ding, B. Mitran, P.H. Edqvist, V. Tolmachev, A. Orlova, T. Gräslund, Affibody-derived drug conjugates: potent cytotoxic molecules for treatment of HER2 over-expressing tumors, J. Control. Release 288 (2018) 84–95.
[75] C.T. Mendler, A. Feuchtinger, I. Heid, M. Aichler, C. D'Alessandria, S. Pirsig, B. Blechert, H.J. Wester, R. Braren, A. Walch, A. Skerra, M. Schwaiger, Tumor uptake of anti-CD20 Fabs depends on tumor perfusion, J. Nucl. Med. 57 (2016) 1971–1977.
[76] M.M. Rinschen, P.F. Huesgen, R.E. Koch, The podocyte protease web: uncovering the gatekeepers of glomerular disease, Am. J. Physiol. Renal Physiol. 315 (2018) F1812–F1816.
[77] N. Kamaly, J.C. He, D.A. Ausiello, O.C. Farokhzad, Nanomedicines for renal disease: current status and future applications, Nat Rev. Nephrol. 12 (2016) 738–753.
[78] C.H. Choi, J.E. Zuckerman, P. Webster, M.E. Davis, Targeting kidney mesangium by nanoparticles of defined size, Proc. Natl. Acad. Sci. U. S. A. 108 (2011) 6656–6661.
[79] C.P. Liu, Y. Hu, J.C. Lin, H.L. Fu, L.Y. Lim, Z.X. Yuan, Targeting strategies for drug delivery to the kidney: from renal glomeruli to tubules, Med. Res. Rev. 39 (2019) 561–578.
[80] D. Schlondorff, The glomerular mesangial cell: an expanding role for a specialized pericyte, FASEB J. 1 (1987) 272–281.